

Source Reconstruction for Spatio-Temporal Physical Statistical Models

Connie Okasaki*

Quantitative Ecology and Resource Management Program, U of Washington,
Mevin B. Hooten

Department of Statistics and Data Sciences, University of Texas at Austin,
and

Andrew M. Berdahl[†]

School of Aquatic and Fisheries Sciences, U of Washington

December 28, 2021

Abstract

In many applications, a signal is deformed by well-understood dynamics before it can be measured. For example, when a pollutant enters a river, it immediately begins dispersing, flowing, settling, and reacting. If the pollutant enters at a single point, its concentration can easily be measured before it enters the complex dynamics of the river system. However, in the case of a non-point source pollutant, it is not clear how to efficiently measure its source. We could record concentration measurements in the river, but this signal is masked by the fluid dynamics of the river. Specifically, concentration is governed by the advection-diffusion-reaction PDE, with an unknown source term. We propose a method to statistically reconstruct a source term from these PDE-deformed measurements. Our method is general and applies to any linear PDE. This method has important applications in the study of environmental DNA and non-point source pollution.

*This material is based upon work supported by the National Science Foundation Graduate Research Fellowship under Grant No. DGE-1762114

[†]AMB was supported by the H. Mason Keeler Endowed Professorship in Sports Fisheries Management.

Keywords: Inverse Problems, GMRF, Gaussian process, Basis function

1 Introduction

In many applications, a signal of interest $f(\mathbf{s})$ is deformed by well-understood physical or mathematical dynamics before it can be measured. However, the primary interest may be inferring the original source of that signal, rather than the function $u(\mathbf{s})$ that is actually measured. This is a common problem and statistical, mathematical, and physical analyses are frequently undertaken to solve it both inside (e.g., Bindler et al. 2001, Hopke et al. 1993, Keats et al. 2007) and outside (e.g., Grech et al. 2008, Nelson & Yoon 2000, Yan et al. 2008) the field of environmental science. One particular example of this problem arises when $u(\mathbf{s})$ is the solution to a partial differential equation (PDE) for which $f(\mathbf{s})$ is a source term. We present a method using stochastic PDEs (SPDEs) to calculate the posterior distribution for the source term of a linear PDE from measurements of the PDE solution. These calculations are efficient when the source can be represented as a Gaussian Markov Random Field (GMRF). We demonstrate the use of this method for reconstructing the non-point source of a pollutant (particulate matter less than 2.5 microns in diameter; or PM2.5) carried through the atmosphere in two simulated-data case studies and one real-data case study, using EPA measurements of PM2.5 (US Environmental Protection Agency 2021) and the NOMADS atmospheric model (Rutledge et al. 2006). We make use of the finite element method (FEM) in what follows for spatial derivatives and the finite difference method (FDM) for temporal derivatives.

1.1 Background

Throughout, we assume that the source $f(\mathbf{s}) \sim GP(\mu(\mathbf{s}), k(\mathbf{s}, \mathbf{s}'))$ is a Gaussian process with mean function μ and covariance function k . We assume that $f(\mathbf{s})$ cannot be measured directly, but is nevertheless the primary target of inference. Furthermore, we assume that f can be represented using a Gaussian Markov Random Field (GMRF; for general reference see Rue & Held (2005)) so that for any particular finite set of points \mathbf{s} , $f(\mathbf{s}) \sim \mathcal{N}(\boldsymbol{\mu}(\mathbf{s}), \mathbf{Q}(\mathbf{s}, \mathbf{s})^{-1})$ with a sparse precision matrix \mathbf{Q} . When k is the Matérn covariance function, Lindgren et al. (2011) provided a method for generating \mathbf{Q} for certain half-integer values of the smoothness parameter α . We assume the dynamics are governed by the PDE

$$\frac{\partial u}{\partial t}(\mathbf{s}, t) + \nabla \cdot (\mathbf{v}(\mathbf{s}, t)u(\mathbf{s}, t)) - \nabla \cdot (D\nabla u(\mathbf{s}, t)) + ru(\mathbf{s}, t) = f(\mathbf{s}, t), \quad (1)$$

where D is the diffusion coefficient, r is the decay rate, and $\mathbf{v}(s, t)$ is the advection field, assumed here to be known. If we assume that $f(s, t) = f(\mathbf{s})$ is homogeneous in time and that $u(s, t) = u(\mathbf{s})$ has reached steady state, the PDE simplifies to

$$\nabla \cdot (\mathbf{v}(\mathbf{s})u(\mathbf{s})) - \nabla \cdot (D\nabla u(\mathbf{s})) + ru(\mathbf{s}) = f(\mathbf{s}). \quad (2)$$

Our methodology can be applied for any linear PDE, and we loosen this assumption using more general partial differential operators in the Appendix. Neumann boundary conditions are the natural boundary conditions (i.e., are automatically satisfied) when applying the conventional finite element method to this equation. We use these boundary conditions throughout but Dirichlet boundary conditions could also be used, as could non-zero Neumann boundary conditions and Robin boundary conditions. Boundary conditions may also be specified in terms of lower-dimensional random fields (see Appendix for details).

1.2 Discretization

Historically, spatial statistical theory has focused on special cases such as isotropic or stationary covariance functions. These models have seen the most detailed analysis as well as the most applications. They also have strong connections to splines and smoothing methods (Miller et al. 2020). However, these relatively simple models are potentially inappropriate when mechanisms are known which violate the core assumptions of isotropy and stationarity. We provide a general purpose solution to this problem when mechanisms can be described by linear dynamics.

We focus our attention specifically on differential equation dynamics, in particular partial differential equations (PDEs), starting with the steady-state advection-diffusion-reaction equation (2). In general, discretization methods translate this equation into a system of linear equations

$$\mathbf{K}\mathbf{u} = \mathbf{L}\mathbf{f}. \quad (3)$$

In the finite element method, \mathbf{K} is known as the stiffness matrix and \mathbf{L} is known as the mass matrix. In the finite difference method, often $\mathbf{L} = \mathbf{I}$ and we have only a matrix on the left-hand side. Essential boundary conditions (i.e., those that are not automatically satisfied; usually Dirichlet) modify this basic equation. We demonstrate this modification in the Appendix. We refer to \mathbf{u} as the solution vector and \mathbf{f} as the source vector.

Our methodology for generating a sparse precision matrix \mathbf{Q}_u given \mathbf{Q}_f is essentially the same as in Lindgren et al. (2011). Their precision matrix recursion can be derived by noting that $\mathbf{u} = \mathbf{K}^{-1}\mathbf{L}\mathbf{f}$, so that if \mathbf{f} is multivariate normal with covariance matrix \mathbf{Q}^{-1} then

\mathbf{u} is multivariate normal with covariance matrix $\mathbf{K}^{-1}\mathbf{L}\mathbf{Q}^{-1}\mathbf{L}\mathbf{K}^{-T}$, and therefore precision matrix $\mathbf{K}\mathbf{L}^{-1}\mathbf{Q}\mathbf{L}^{-1}\mathbf{K}^T$. Caveats occur in several cases, notably if \mathbf{K} is singular, and in certain circumstances when the finite element equation $\mathbf{u} = \mathbf{K}^{-1}\mathbf{L}\mathbf{f}$ does not converge to the true solution, such as in the case of naïvely-implemented electromagnetic FEMs (Monk et al. 2003), which requires more sophisticated finite elements such as Nédélec elements. For the advection-diffusion equation, the usual concern is the artificial small scale behavior that discretization induces, which can be mitigated using, for example, the streamline-upwind Petrov-Galerkin method (Brooks & Hughes 1982). For our purposes, we ignore undesirable small scale behavior and use linear tetrahedral elements, which suffice to demonstrate our method.

Although the finite difference method would produce conceptually identical results, we use the finite element method to compute discretized spatial derivatives. Because the stiffness and mass matrices are standard components of finite element analysis in engineering, they can be easily calculated by leveraging existing FEM software such as FEniCS (Alnæs et al. 2015). We propose to use physically-motivated SPDEs, while relying on FEM software to implement our stiffness and mass matrices. This allows us to avoid cumbersome analytical calculations while incorporating complex phenomena such as spatially-varying model coefficients. It also improves reproducibility and facilitates generalizability. We assume that the FEM approach is appropriate for any SPDE in which the stochastic source term is well-behaved and in which the FEM equation converges to the true solution in the deterministic case.

2 The Advection-Diffusion-Reaction Equation

2.1 Background

We now consider the advection-diffusion-reaction equation in more detail. Suppose that we seek to infer the source of a chemical, but only have measurements of chemical concentration in a fluid medium. The chemical flows with, and disperses through, that medium, and also decays linearly over time. For example, this model may be appropriate when trying to estimate the origin of non-point source pollution (e.g., runoff pollution); the source of stable isotopes found in water samples; or the biomass of fish from environmental DNA (eDNA) measurements. This inverse problem has been considered in applied math studies, and is usually solved either in the case where the chemical is assumed to originate with unknown strength from a small finite number of unknown point locations (El Badia et al. 2005, El Badia & Hamdi 2007, Lushi & Stockie 2010), or using regularization techniques

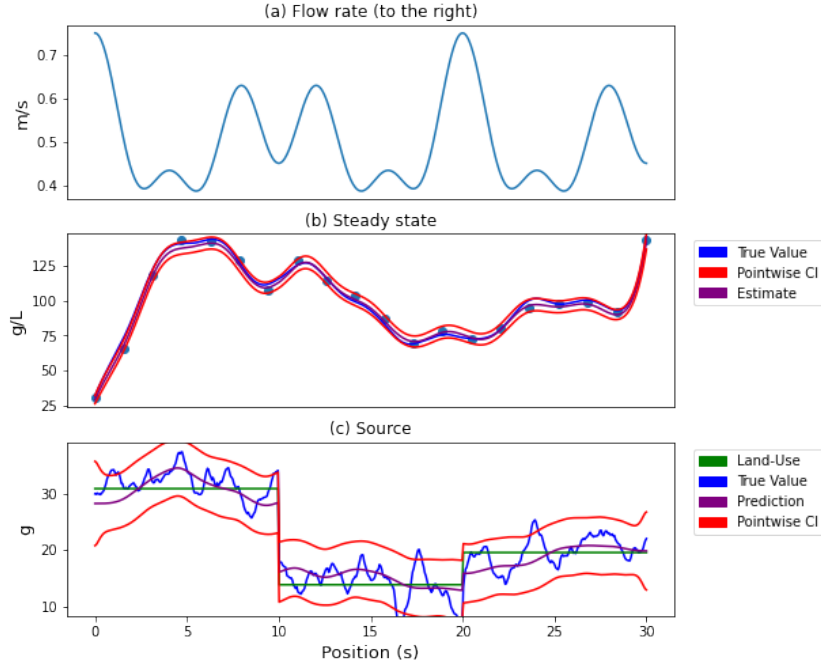


Figure 1: The results of a numerical experiment for conducting source reconstruction on the advection-diffusion-reaction equation, with a linear regression on spatial factors. Panel (a) shows the spatially-variable flow rate (always to the right). Panel (b) shows inference on \mathbf{u} . Panel (c) shows inference on $\mathbf{f} = \mathbf{X}\boldsymbol{\beta} + \boldsymbol{\epsilon}$. Note the discontinuities in \mathbf{f} generated by discontinuities in \mathbf{X} . Also note the spurious oscillations at those discontinuities. Dots show position of measurements and their observed values.

from the inverse problems literature that do not admit a probabilistic interpretation and do not include an estimate of uncertainty (Porter & Devaney 1982, Engl et al. 1996, Yan et al. 2008).

Previous statistical work (Sigrist et al. 2012) has examined the advection-diffusion equation in an SPDE context using spectral methods, however our approach easily extends to the case where the flow, diffusion, and decay rates are not constant in space, or the domain is irregularly shaped, as is common when domains are defined based on GIS data. Stroud et al. (2010) uses the finite difference method to account for these practicalities but uses an ensemble Kalman filter method to conduct inference, rather than approaching the problem from an SPDE perspective.

3 Case Studies

3.1 Case Study 1: Steady State, One Dimension, Covariates

For this case study, suppose we make measurements of runoff pollution $u(s)$ at various points in a 1-D stream. The land alongside the stream may be used for several different purposes; for example, it may be agricultural, residential, or industrial. The primary source of variation in pollutant source $f(s)$ may be due to variations in land use (represented by a factor variable), so that $f(s) = \mathbf{x}(s)^T \boldsymbol{\beta} + \epsilon(s)$ where ϵ can be represented as a mean-zero GMRF and $\boldsymbol{\beta}$ has a normal prior. We find the joint posterior for \mathbf{f} and $\boldsymbol{\beta}$ based on measurements of \mathbf{u} by first calculating the joint posterior of \mathbf{u} and $\boldsymbol{\beta}$ and then applying the finite element equation to obtain \mathbf{f} . Figure 1 shows the results of this analysis, with three land-use zones applying differing constant contributions to the source. The sharp discontinuities due to differing land use generate the small scale behavior characteristic of FEM models of advection, but this has a minor effect on the final results in practice. This case study showcases the ability to incorporate linear regression into our method and to efficiently obtain analytical conditional distributions when dynamics are perfectly known. We will use these conditional distributions to marginalize out \mathbf{u} and \mathbf{f} in the next section, when we use MCMC to fit the model.

3.2 Case Study 2: Steady State, Two Dimensions, Real Data

We implemented the steady-state advection-diffusion-reaction equation to conduct source inference on PM2.5 over the United States for January 1st 2019. We obtained the PM2.5 data from the EPA (US Environmental Protection Agency 2021) and parameterized our wind-speed data using NOMADS (Rutledge et al. 2006). We assumed a homogeneous prior mean for \mathbf{f} , although population density, automobile density, land use, or many other covariates could also be included. We included a buffer region of approximately 4 degrees on all sides, and projected locations from degrees latitude/longitude to kilometers, preserving the distance between longitudes at all latitudes. We also projected advection velocities to ensure that the travel time between two points was preserved, although distances between two points and advection speeds were in general not preserved.

We assumed that the emissions (source function; $f(\mathbf{s})$) were governed by a Matérn Gaussian process and that the variance and range of this process were unknown, along with the diffusion and decay coefficients. We fit this model using a custom Metropolis-Hastings MCMC algorithm. We specified an inverse-gamma prior for σ_f^2 the variance of the emissions function, to facilitate Gibbs sampling, and we specified gamma priors for ρ, v, D ,

Parameter	Posterior Mean	Posterior Std. Dev.	Prior	Prior Quantiles (.025,.975)
ρ	48.7 km	3.5 km	$\alpha = 4, \beta = 0.1$	(10,80)
D	8.0 km ² /hr	2.7 km ² /hr	$\alpha = 8.5, \beta = 1$	(3.6,14.4)
r	1.41/hr	0.47/hr	$\alpha = 1.36, \beta = 2.94$	(0.027,1.5)
σ_f^2	159 ($\mu\text{g}/\text{m}^3$) ²	115 ($\mu\text{g}/\text{m}^3$) ²	$\alpha = 1.1, \beta = 3.9$	(1,100)
v	0.31	0.24	$\alpha = 1.1, \beta = 0.13$	(0.33,30)
σ_ϵ^2	31.5 ($\mu\text{g}/\text{m}^3$) ²	1.8 ($\mu\text{g}/\text{m}^3$) ²	NA	NA
σ_f	11.9 $\mu\text{g}/\text{m}^3$	4.1 $\mu\text{g}/\text{m}^3$	NA	NA
σ_ϵ	5.61 $\mu\text{g}/\text{m}^3$	0.16 $\mu\text{g}/\text{m}^3$	NA	NA

Table 1: Fitted parameter values for the advection-diffusion-reaction source model.

and r (respectively, the range; ratio of observation variance σ_ϵ^2 to emissions variance σ_f^2 ; diffusion coefficient; and decay coefficient). To use the range as a parameter we used the empirical equation $\rho = \sqrt{8\nu/\kappa}$ which relates range to the Matérn parameters and transformed the log-likelihood accordingly. To use Gibbs sampling for σ_f^2 we reparameterized to the variance ratio: $v = \frac{\sigma_\epsilon^2}{\sigma_f^2}$. Again we transformed the log-likelihood accordingly. We specified mild priors based on existing literature (ρ (Song et al. 2018); D (Byun & Schere 2006); r (Watson et al. 2000, Cao et al. 2013); σ_f^2 (Tucker 2000); v (Peters et al. 2001)) and understanding of the mechanisms involved. Due to the identifiability problems with the Matérn α parameter (Lindgren et al. 2011), we assumed *a priori* that $\alpha = 2$ and therefore $\nu = 1$, and that the prior mean of f was everywhere zero. Prior parameters and quantiles, and posterior statistics can be found in Table 1.

When conducting MCMC we marginalized over the concentration and emission vectors \mathbf{u} and \mathbf{f} , but used a second-stage algorithm to sample from the full-conditional distributions of \mathbf{u} and \mathbf{f} to compute their posterior means and pointwise standard deviations. MCMC plots and diagnostics can be found in the appendix. We ran 4 samplers for 5,000 iterations each, with a thinning rate of 5.

The main components and results of this analysis can be found in Figure 2. Uncertainty was quantified using the square root of the diagonal elements of the dense posterior covariance matrix (i.e. the pointwise posterior standard deviations). Posterior uncertainty was lower around the main landmass of the continental US, because this is where the data were collected, and regions of high estimated emissions and concentration were clustered around some regions of high population including Texas, California, Florida, and the Pacific Northwest. Some anomalies are present in the results, notably some rare but large negative predictions for PM 2.5 concentrations. These either represent regions that are a net sink

of PM 2.5, or are non-physical predictions that we hypothesize are due to the snapshot-in-time nature of these measurements. Our model assumes the system is in steady-state, thus it must also assume the advection rate is constant in time. Because weather systems move over time, we hypothesize these negative predictions may be due to the steady-state assumption. If concentrations are low in a region that simultaneously has low wind speed, the steady state model assumes that wind speed has always been low, and that the low concentration reflects the end result of a build-up of concentration over time. Because this build-up would normally result in a region of very high concentration, the model must conclude that there is a nearby region of negative concentration to balance the system. This phenomenon may not occur in a space-time version of this model. For similar reasons, several regions were predicted to have higher concentrations than any sampled data point. This may be due to a similar phenomenon (high concentrations measured in several areas nearby to a confluence of wind speeds); or may be due to the weighted-average nature of a finite element model (i.e., a higher than average measurement on the outskirts of a city, where it is known with a high degree of confidence that concentration is lower inside the city, is modeled as the result of a weighted average between a high-concentration node outside the city, and a low-concentration node inside the city).

The units of emissions are $\mu\text{g}/\text{m}^3/\text{hour}$. We prefer emissions to be measured in μg directly. However, doing so would require making a homogeneity assumption to account for the vertical distribution of PM2.5 (we use this approach to approximate a prior distribution for σ_T^2), or directly modeling vertical distribution with a fully 3-D model. Such a model is not difficult to mesh using FEniCS but is much larger and more computationally intensive, and we leave this extension for future work.

3.3 Case Study: 1-D, Time-Dependent

Thus far we have assumed steady-state PDEs, and in the previous section we saw the potential advantages of including time-dependence. Although the steady-state assumption will sometimes be necessary due to the computationally-intensive nature of spatio-temporal modeling, adding in a temporal component may improve the performance of the model. Our implementation of time-dependence relies on a finite element method in space and a finite difference method in time. As in Wikle & Hooten (2010), this results in a sparse vector auto-regressive (VAR) model for the spatial variables. Suppose, for example, that we wish to analyze the full time-dependent advection-diffusion-reaction equation (1). For a small time interval Δt , a backward Euler discretization in time, coupled to the FEM

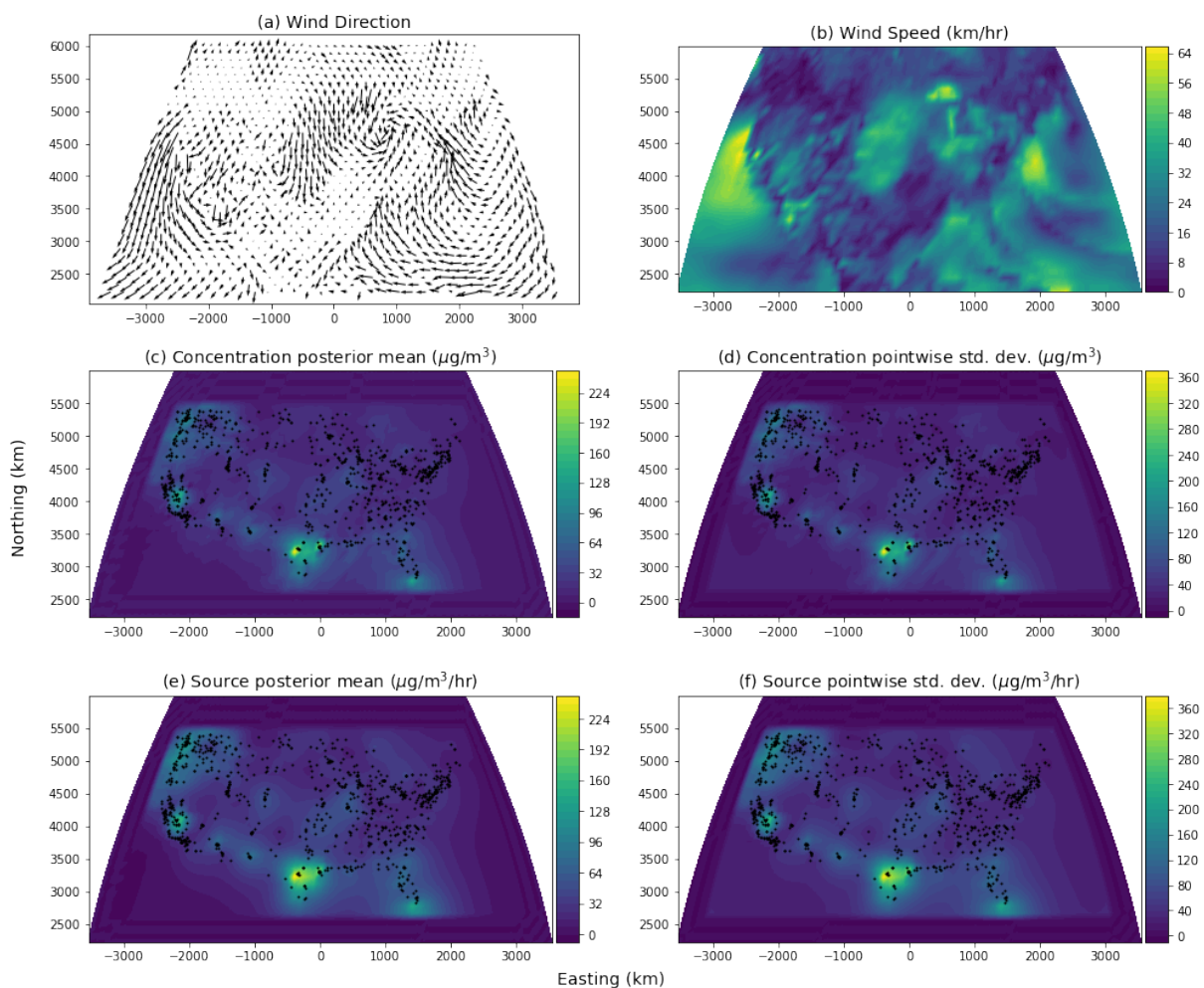


Figure 2: The main results of our real-data case study, parameterized with the NOMADs climate model (Rutledge et al. 2006), and using EPA PM 2.5 measurements (US Environmental Protection Agency 2021). Advection field (a; upper left); advection speed (b; upper right); PM 2.5 map (c; middle left); PM 2.5 map posterior standard deviation (d; middle right); PM 2.5 emissions map (e; lower left); PM 2.5 source map posterior standard deviation (f; lower right). The buffer region (approximately 4 degrees wide) is set to zero to avoid showing boundary anomalies. Dots represent locatins of data points.

discretization in space, yields:

$$\mathbf{u}_{t+\Delta t} = \mathbf{u}_t + \Delta t \mathbf{f}_{t+\Delta t} - \mathbf{L}^{-1} \mathbf{K}_{t+\Delta t} \mathbf{u}_{t+\Delta t} \quad (4)$$

$$= (\mathbf{I} + \mathbf{L}^{-1} \mathbf{K})^{-1} (\mathbf{u}_t + \Delta t \mathbf{f}_{t+\Delta t}) \quad (5)$$

which inductively is solved by

$$\begin{bmatrix} \mathbf{u}_1 \\ \mathbf{u}_2 \\ \vdots \\ \mathbf{u}_N \end{bmatrix} = \begin{bmatrix} \mathbf{M} \\ \mathbf{M}^2 \\ \vdots \\ \mathbf{M}^N \end{bmatrix} \mathbf{u}_0 + \Delta t \begin{bmatrix} \mathbf{M}_1 & & & & \\ \mathbf{M}_2 \mathbf{M}_1 & \mathbf{M}_2 & & & \\ \mathbf{M}_3 \mathbf{M}_2 \mathbf{M}_1 & \mathbf{M}_3 \mathbf{M}_2 & \mathbf{M}_3 & & \\ \vdots & \vdots & \vdots & \ddots & \\ \mathbf{M}_N \dots \mathbf{M}_1 & \mathbf{M}_N \dots \mathbf{M}_2 & \dots & \dots & \mathbf{M}_N \end{bmatrix} \begin{bmatrix} \mathbf{f}_1 \\ \mathbf{f}_2 \\ \vdots \\ \mathbf{f}_N \end{bmatrix}, \quad (6)$$

where $\mathbf{M} = (\mathbf{I} + \mathbf{L}^{-1} \mathbf{K})^{-1}$. The above Toeplitz matrix has sparse inverse

$$\mathbf{R} = \frac{1}{\Delta t} \begin{bmatrix} \mathbf{M}_1 & & & & \\ -\mathbf{I} & \mathbf{M}_2 & & & \\ & -\mathbf{I} & \mathbf{M}_3 & & \\ & & \ddots & \ddots & \\ & & & -\mathbf{I} & \mathbf{M}_3 \end{bmatrix}. \quad (7)$$

A forward Euler discretization yields a very similar matrix, but requires that the time step Δt is small enough that \mathbf{R} remains positive semi-definite.

Suppose that the full, discretized, spatio-temporal process \mathbf{f} has sparse precision matrix \mathbf{Q}_f and that we have a deterministic initial condition $\mathbf{u}_0 = \mathbf{0}$ (accounted for by including a temporal buffer region before the region of interest). Then the precision matrix for \mathbf{u} is

$$\mathbf{Q}_u = \mathbf{R}^T \mathbf{Q}_f \mathbf{R}. \quad (8)$$

Our initial condition requires us to extend the temporal discretization prior to the first time-of-interest, to avoid boundary effects. Alternatively, the steady-state equation could be used to derive an approximate spatial prior for the initial condition, although this should still be coupled with a buffer region.

3.3.1 Spatio-temporal Matérn

The need for a non-mechanistic spatio-temporal source distribution compatible with our method motivates the following definition of a three-parameter spatio-temporal Matérn

field

$$\left(\tau \frac{\partial}{\partial t} + \kappa^2 - \Delta\right)^{\alpha/2} u(\mathbf{s}, t) = \mathcal{W}(\mathbf{s}, t). \quad (9)$$

This is a nested spatio-temporal diffusion equation, and if we define the source term as constant-in-time spatial white noise $\mathcal{W}(x)$ then the spatial Matérn SPDE is the steady state solution. Although the Matérn model does not necessarily require interpretation, the interpretation of this nested diffusion model is more straightforward than an alternative model for which the spatial Matérn SPDE is also the steady state solution

$$\tau \frac{\partial u}{\partial t}(\mathbf{s}, t) + (\kappa^2 - \Delta)^{\alpha/2} u(\mathbf{s}, t) = \mathcal{W}(\mathbf{s}, t). \quad (10)$$

To avoid fractional diffusion we must assume $\alpha = 2n$ for $n \in \mathbb{Z}_{>0}$, for which we obtain

$$\mathbf{Q}_u^{(2n)} = \frac{\mathbf{R}^{Tn}}{\Delta t} (\mathbf{L} \otimes \mathbf{I}) \frac{\mathbf{R}}{\Delta t}. \quad (11)$$

This results in $\mathbf{Q}_f = \mathbf{L} \otimes \mathbf{I}$, which is straightforward to calculate. For example, Figure 3 shows the results of a numerical simulation of this distribution. Although a spatial buffer-zone was included in these calculations and removed from the plot, the temporal buffer-zone was not removed, to demonstrate the transient behavior imposed by our deterministic initial condition. A small zone with length on the order τ displays lower spatio-temporal variance than the remainder of the plot, but no differences appear to persist beyond that. For this set of parameters, we used $\Delta t = 3 \times 10^{-3}$ and 10^4 time steps. With 751 spatial nodes, simulation required less than 1 second on a desktop computer with a 3.2 GHz 6-core processor and 32 GB of RAM.

3.3.2 Case Study 3: Spatio-temporal, 1-D

Suppose that we wish to apply our source-reconstruction method in space-time. This requires us to conduct our analysis in a high-dimensional spatio-temporal space. Nevertheless, analysis remains feasible due to the efficiency of sparse matrix calculations. Figure 4 shows the results of analysis in 1 spatial dimension and 1 temporal dimension. We simulated the advection diffusion equation with a spatio-temporal Matérn source as defined in equation (9). We simulated 5 sensors equidistant along the s -axis, and simulated 10 measurements each, equidistant in time.

The solution (concentration) estimate is more accurate than the source estimate, because this is the scale at which we are able to take direct measurements, while the source

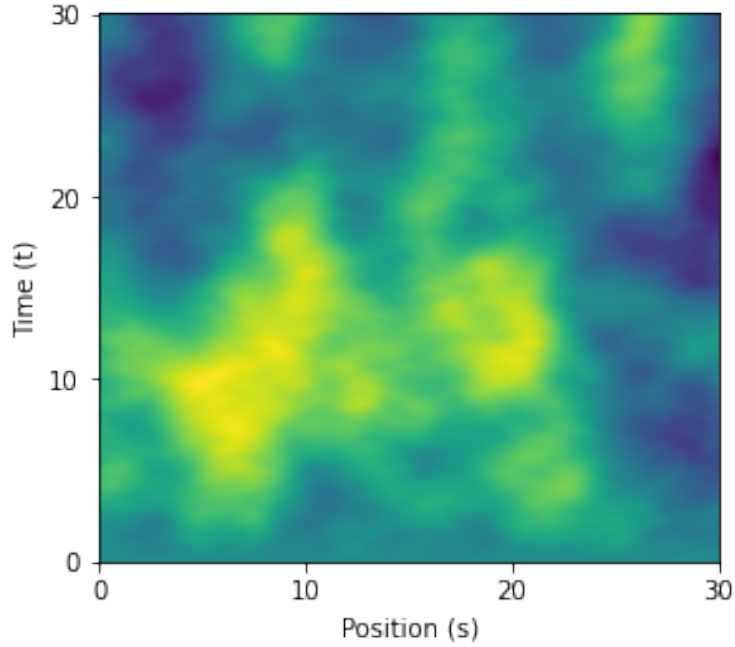


Figure 3: The results of a numerical simulation of the proposed spatio-temporal Matérn distribution. Parameters used were: $\tau = 1, \alpha = 4, \kappa = 0.06$. A spatial buffer zone of length 5 on each side is not included in the plot. No temporal buffer zone was removed. Space-time was discretized using 751 spatial nodes, and 10^4 time steps.

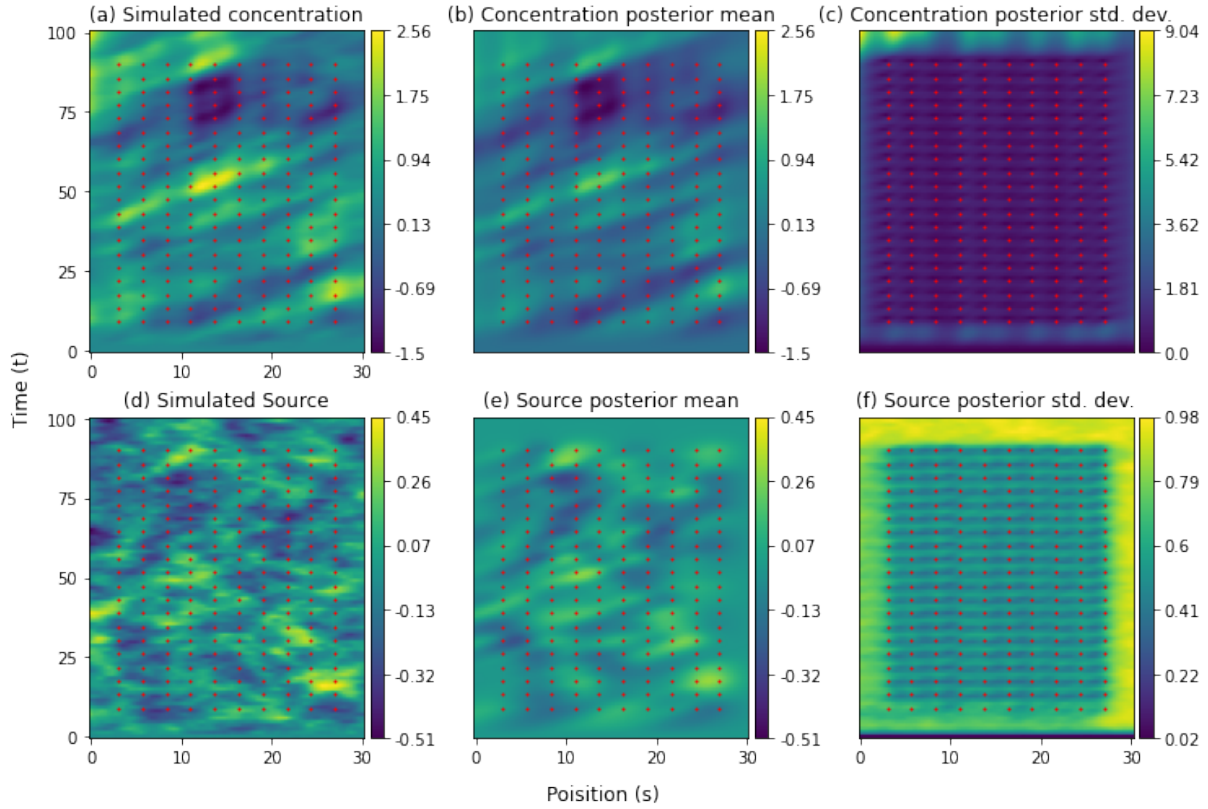


Figure 4: The results of Case Study 3. The source process was spatio-temporal Matérn as defined in Section 3.3.1 with parameters: $\tau = 1, \alpha = 4, \kappa = 0.06$. Flow rate was constant in time, and varied in space as shown in figure 1. Red points denote sampling locations. A spatial buffer zone of length 5 on each side is not included in the plot. No temporal buffer zone was removed.

reconstruction displays a greater degree of smoothing due to the obscuring effects of diffusion and advection. Because the material detected in a concentration measurement could have originated from any point nearby or upstream, a larger number of measurements are required to provide equivalent resolution on the source function. As more measurements are recorded, the reconstruction converges to the simulated source. Our method can be thought of as a filter that treats concentration measurements as an integral over previous, mostly upstream sources. That is, a measurement of concentration at time t only provides information about the source process up to time t , and provides much stronger information from upstream locations (due to advection) than from downstream locations (due to diffusion). Any information about future or downstream source values is contained only in the correlation structure of the source process. Figure 4 panel (f) demonstrates this behavior on its margins, where downstream and future uncertainties are higher than upstream and past uncertainties.

4 Conclusion

We presented a method for SPDE-based inference on the source of a linear process, in this case a PDE. We demonstrated this method for reconstructing an advection-diffusion-reaction source function in a 1-D simulated case study, a 2-D real data case study, and a 1-D spatio-temporal simulated case study. Possible applications include inferring the source of environmental DNA measurements, non-point source pollution, or stable isotopes, and inferring the form of a dynamical system. Other important linear PDEs include Maxwell’s equations and the wave equation. Using these equations, our method could be applied to MRI measurements or earthquake reconstruction. Our approach uses an SPDE method similar to Lindgren et al. (2011) to solve this problem in a Bayesian framework, providing the opportunity to explicitly incorporate linear regression models on the source function, and to calculate the uncertainty of our solution, in contrast to most existing “inverse problems” approaches. By incorporating our methodology and source-inference perspective into existing hierarchical frameworks (Wikle & Hooten 2010), process uncertainty and non-Gaussian observations can also be accommodated.

References

Alnæs, M., Blechta, J., Hake, J., Johansson, A., Kehlet, B., Logg, A., Richardson, C., Ring, J., Rognes, M. E. & Wells, G. N. (2015), ‘The FEniCS project version 1.5’, *Archive of*

Numerical Software **3**(100).

- Bindler, R., Renberg, I., Anderson, N. J., Appleby, P. G., Emteryd, O. & Boyle, J. (2001), ‘Pb isotope ratios of lake sediments in West Greenland: Inferences on pollution sources’, *Atmospheric Environment* **35**(27), 4675–4685.
- Brooks, A. N. & Hughes, T. J. (1982), ‘Streamline upwind/Petrov-Galerkin formulations for convection dominated flows with particular emphasis on the incompressible Navier-Stokes equations’, *Computer Methods in Applied Mechanics and Engineering* **32**(1-3), 199–259.
- Byun, D. & Schere, K. L. (2006), ‘Review of the governing equations, computational algorithms, and other components of the Models-3 Community Multiscale Air Quality (CMAQ) modeling system’, *Applied Mechanics Reviews* **59**(2), 51–77.
- Cao, J., Chow, J. C., Lee, F. S., Watson, J. G. et al. (2013), ‘Evolution of PM_{2.5} measurements and standards in the US and future perspectives for China’, *Aerosol and Air Quality Research* **13**(4), 1197–1211.
- El Badia, A., Ha-Duong, T. & Hamdi, A. (2005), ‘Identification of a point source in a linear advection–dispersion–reaction equation: Application to a pollution source problem’, *Inverse Problems* **21**(3), 1121.
- El Badia, A. & Hamdi, A. (2007), ‘Inverse source problem in an advection-dispersion-reaction system: Application to water pollution’, *Inverse Problems* **23**(5), 2103.
- Engl, H. W., Hanke, M. & Neubauer, A. (1996), *Regularization of Inverse Problems*, Vol. 375, Springer Science & Business Media.
- Grech, R., Cassar, T., Muscat, J., Camilleri, K. P., Fabri, S. G., Zervakis, M., Xanthopoulos, P., Sakkalis, V. & Vanrumste, B. (2008), ‘Review on solving the inverse problem in EEG source analysis’, *Journal of Neuroengineering and Rehabilitation* **5**(1), 25.
- Hopke, P. K., Gao, N. & Cheng, M.-D. (1993), ‘Combining chemical and meteorological data to infer source areas of airborne pollutants’, *Chemometrics and Intelligent Laboratory Systems* **19**(2), 187–199.
- Keats, A., Yee, E. & Lien, F.-S. (2007), ‘Bayesian inference for source determination with applications to a complex urban environment’, *Atmospheric Environment* **41**(3), 465–479.

- Lindgren, F., Rue, H. & Lindström, J. (2011), ‘An explicit link between Gaussian fields and Gaussian Markov random fields: the stochastic partial differential equation approach’, *Journal of the Royal Statistical Society: Series B (Statistical Methodology)* **73**(4), 423–498.
- Lushi, E. & Stockie, J. M. (2010), ‘An inverse Gaussian plume approach for estimating atmospheric pollutant emissions from multiple point sources’, *Atmospheric Environment* **44**(8), 1097–1107.
- Miller, D. L., Glennie, R. & Seaton, A. E. (2020), ‘Understanding the stochastic partial differential equation approach to smoothing’, *Journal of Agricultural, Biological and Environmental Statistics* **25**(1), 1–16.
- Monk, P. et al. (2003), *Finite element methods for Maxwell’s equations*, Oxford University Press.
- Nelson, P. A. & Yoon, S.-H. (2000), ‘Estimation of acoustic source strength by inverse methods: Part I, conditioning of the inverse problem’, *Journal of Sound and Vibration* **233**(4), 639–664.
- Peters, T. M., Norris, G. A., Vanderpool, R. W., Gemmill, D. B., Wiener, R. W., Murdoch, R. W., Mcelroy, F. F. & Pitchford, M. (2001), ‘Field performance of PM_{2.5} federal reference method samplers’, *Aerosol Science & Technology* **34**(5), 433–443.
- Porter, R. P. & Devaney, A. J. (1982), ‘Holography and the inverse source problem’, *Journal of the Optical Society of America* **72**(3), 327–330.
- Rue, H. & Held, L. (2005), *Gaussian Markov Random Fields: Theory and Applications*, CRC Press.
- Rutledge, G. K., Alpert, J. & Ebisuzaki, W. (2006), ‘NOMADS: A climate and weather model archive at the National Oceanic and Atmospheric Administration’, *Bulletin of the American Meteorological Society* **87**(3), 327–342.
- Sigrist, F., Künsch, H. R. & Stahel, W. A. (2012), ‘A dynamic nonstationary spatio-temporal model for short term prediction of precipitation’, *The Annals of Applied Statistics* pp. 1452–1477.

- Song, W., Jia, H., Li, Z. & Tang, D. (2018), ‘Using geographical semi-variogram method to quantify the difference between NO₂ and PM_{2.5} spatial distribution characteristics in urban areas’, *Science of the Total Environment* **631**, 688–694.
- Stroud, J. R., Stein, M. L., Lesht, B. M., Schwab, D. J. & Beletsky, D. (2010), ‘An ensemble Kalman filter and smoother for satellite data assimilation’, *Journal of the American Statistical Association* **105**(491), 978–990.
- Tucker, W. G. (2000), ‘An overview of PM_{2.5} sources and control strategies’, *Fuel Processing Technology* **65**, 379–392.
- US Environmental Protection Agency (2021), ‘Air Quality System Data Mart’, Internet Database available at <http://www.epa.gov/ttn/airs/aqsdatamart>. Accessed: 2021-02-24.
- Watson, J. G., Chow, J. C. & Pace, T. G. (2000), ‘Fugitive dust emissions’, *Crops* **3**(14), 7.
- Wikle, C. K. & Hooten, M. B. (2010), ‘A general science-based framework for dynamical spatio-temporal models’, *Test* **19**(3), 417–451.
- Yan, L., Fu, C.-L. & Yang, F.-L. (2008), ‘The method of fundamental solutions for the inverse heat source problem’, *Engineering Analysis with Boundary Elements* **32**(3), 216–222.

5 Appendix

5.1 General Operator

A more general formulation can be expressed as

$$\mathcal{L}u(x) = f(x), \quad \forall x \in \Omega \quad (12)$$

$$b(u(x), \nabla u(x)) = c(x), \quad \forall x \in \partial\Omega \quad (13)$$

where \mathcal{L} is a second-order partial differential operator and b is some function representing a boundary condition.

5.2 Dirichlet Boundary Conditions

Although Neumann boundary conditions on \mathbf{u} are most common, Dirichlet boundary conditions on \mathbf{u} can be incorporated into our approach, as can boundary conditions on \mathbf{f} . Using the basic FEM method, Neumann boundary conditions are considered “natural,” that is, the solution to $\mathbf{K}\mathbf{u} = \mathbf{L}\mathbf{f}$ will satisfy these BCs without any additional input. On the other hand Dirichlet boundary conditions are considered “essential,” meaning that we must impose these externally. Note that more sophisticated FEM methods may have different natural/essential BCs, so that these terms are not simply synonymous with Neumann/Dirichlet.

To demonstrate how to incorporate Dirichlet boundary conditions, suppose that our basic Neumann BC generates the FEM formula

$$\mathbf{K}\mathbf{u} = \mathbf{L}\mathbf{f} \quad (14)$$

Our Dirichlet boundary condition can be expressed by splitting \mathbf{u} into component vectors $\mathbf{u}_{\partial\Omega}$ or \mathbf{u}_1 and \mathbf{u}_Ω or \mathbf{u}_2 representing the internal and external degrees of freedom (i.e., nodes/basis functions in our cases). This makes our FEM equation

$$\begin{bmatrix} \mathbf{K}_{11} & \mathbf{K}_{12} \\ \mathbf{K}_{21} & \mathbf{K}_{22} \end{bmatrix} \begin{bmatrix} \mathbf{u}_1 \\ \mathbf{u}_2 \end{bmatrix} = \begin{bmatrix} \mathbf{L}_{11} & \mathbf{L}_{12} \\ \mathbf{L}_{21} & \mathbf{L}_{22} \end{bmatrix} \begin{bmatrix} \mathbf{f}_1 \\ \mathbf{f}_2 \end{bmatrix}. \quad (15)$$

To impose a Dirichlet boundary condition of the form $\mathbf{B}\mathbf{u}_{\partial\Omega} = \mathbf{c}$, we replace the first block-rows of this equation

$$\begin{bmatrix} \mathbf{B} & \mathbf{0} \\ \mathbf{K}_{21} & \mathbf{K}_{22} \end{bmatrix} \begin{bmatrix} \mathbf{u}_1 \\ \mathbf{u}_2 \end{bmatrix} = \begin{bmatrix} \mathbf{I} & \mathbf{0} \\ \mathbf{L}_{21} & \mathbf{L}_{22} \end{bmatrix} \begin{bmatrix} \mathbf{c} \\ \mathbf{f}_2 \end{bmatrix}. \quad (16)$$

The first set of equations determines \mathbf{u}_1 , assuming that \mathbf{B} is invertible. Then we are left with

$$\mathbf{K}_{21}\mathbf{u}_1 + \mathbf{K}_{22}\mathbf{u}_2 = \mathbf{L}_{21}\mathbf{c} + \mathbf{L}_{22}\mathbf{f}_2. \quad (17)$$

Assuming that \mathbf{c} is a constant vector, we are left with a simple offset to the mean of \mathbf{u}_2 , i.e.,

$$\mathbf{u}_2 = \boldsymbol{\mu} + \mathbf{K}_{22}^{-1}\mathbf{L}_{22}\mathbf{f}_2, \quad (18)$$

$$\boldsymbol{\mu} = \mathbf{L}_{21}\mathbf{c} - \mathbf{K}_{21}\mathbf{u}_1 \quad (19)$$

$$= (\mathbf{L}_{21} + \mathbf{K}_{21}\mathbf{B}^{-1})\mathbf{c}, \quad (20)$$

In the event that $\mathbf{c} = \mathbf{0}$, this offset is also $\mathbf{0}$ and we are left with a lower-dimensional version of the same FEM equation. In the event that \mathbf{c} is itself a lower-dimensional GMRF rather than a constant, then instead of a mean offset, this results in a more complex Gaussian random field with covariance

$$(\mathbf{L}_{21} + \mathbf{K}_{21}\mathbf{B}^{-1})\boldsymbol{\Sigma}_c(\mathbf{L}_{21} + \mathbf{K}_{21}\mathbf{B}^{-1})^T + \mathbf{K}_{22}^{-1}\mathbf{L}_{22}\boldsymbol{\Sigma}_{f_2}\mathbf{L}_{22}^T\mathbf{K}_{22}^{-T}, \quad (21)$$

This can be inverted using the Woodbury matrix formula, giving us

$$\mathbf{Q}_{f_1} = \mathbf{Q}_{f_2} - \mathbf{Q}_{f_2}(\mathbf{L}_{21} + \mathbf{K}_{21}\mathbf{B}^{-1})(\mathbf{Q}_c + (\mathbf{L}_{21} + \mathbf{K}_{21}\mathbf{B}^{-1})^T\mathbf{Q}_{f_2}(\mathbf{L}_{21} + \mathbf{K}_{21}\mathbf{B}^{-1}))^{-1}(\mathbf{L}_{21} + \mathbf{K}_{21}\mathbf{B}^{-1})^T\mathbf{Q}_{f_2}. \quad (22)$$

With the simplifying assumption that we replace \mathbf{L} with $\tilde{\mathbf{L}}$, we arrive at $\mathbf{L}_{21} = \mathbf{0}$ so that we obtain

$$\tilde{\mathbf{Q}}_{f_2} = \mathbf{Q}_{f_2} - \mathbf{Q}_{f_2}\mathbf{K}_{21}\mathbf{B}^{-1}(\mathbf{Q}_c + \mathbf{K}_{21}^T\mathbf{B}^{-T}\mathbf{Q}_{f_2}\mathbf{B}^{-1}\mathbf{K}_{21})^{-1}\mathbf{B}^{-1}\mathbf{K}_{21}^T\mathbf{Q}_{f_2}. \quad (23)$$

Assuming that \mathbf{c} is much lower-dimensional than \mathbf{f}_1 , this may be Cholesky decomposed by first decomposing \mathbf{Q}_{f_2} and then computing a low-rank update to this decomposition.